

# NJC

Accepted Manuscript



This is an *Accepted Manuscript*, which has been through the Royal Society of Chemistry peer review process and has been accepted for publication.

*Accepted Manuscripts* are published online shortly after acceptance, before technical editing, formatting and proof reading. Using this free service, authors can make their results available to the community, in citable form, before we publish the edited article. We will replace this *Accepted Manuscript* with the edited and formatted *Advance Article* as soon as it is available.

You can find more information about *Accepted Manuscripts* in the [Information for Authors](#).

Please note that technical editing may introduce minor changes to the text and/or graphics, which may alter content. The journal's standard [Terms & Conditions](#) and the [Ethical guidelines](#) still apply. In no event shall the Royal Society of Chemistry be held responsible for any errors or omissions in this *Accepted Manuscript* or any consequences arising from the use of any information it contains.



Journal Name

ARTICLE

## Ionic liquids as modulators of fragrance release in consumer goods

Received 00th January 20xx,  
Accepted 00th January 20xx

DOI: 10.1039/x0xx00000x

www.rsc.org/

Federico M. Ferrero Vallana,<sup>a</sup> Ricardo P. Girling,<sup>b</sup> Lynette A. M. Holland,<sup>b</sup> Pauline McNamee,<sup>b</sup> Kenneth R. Seddon,<sup>a</sup> Jonathan Stonehouse<sup>b</sup> and Oreste Todini<sup>c</sup>

When organic esters or alcohols were dissolved in each of three novel ionic liquids (which have no effective vapour pressure), the vapour-liquid equilibria (as measured by infrared spectroscopy of the gas phase) revealed significant positive deviation from Raoult's law for a wide range of perfume raw materials. The addition of water amplified the repulsive effect of the ionic liquid matrix, and this was exemplified by a series of ternary phase diagrams.

### Introduction

Ionic liquids are a class of salts, consisting typically of a large asymmetrical organic cation and either an organic or inorganic anion. These can be selected and synthesised with a wide variety of structures depending on the specific technology to which they will be applied.<sup>1</sup> One intriguing new potential application for these materials is controlled fragrance release, especially in household products.<sup>2</sup> For example, ionic liquids have been used as "fixatives" with fragrance compositions to lower the rate of evaporation of a perfume component, or to impart increased stability/longevity of the fragrance.<sup>3</sup> Recently, ionic liquids have also been used as pro-fragrances, where a perfume raw material has been appended covalently to either the cation or the anion,<sup>4</sup> and for the synthesis of floral notes such as  $\delta$ -damascone, which is widely used in the detergent industry.<sup>5</sup> Elsewhere, Forsyth *et al.*<sup>6</sup> investigated the utilisation of ionic liquids for the synthesis of the Lily-of-the-Valley fragrance { $\beta$ -Lilial<sup>®</sup>; 3-(4-*t*-butylphenyl)-2-methylpropanal}.

Fragrances are added to many successful consumer goods in order to impart a long-lasting, pleasant, and product-appropriate odour.<sup>7</sup> The perception of this odour depends upon the concentration and nature of the fragrance molecule released into the air. The design of selective and efficient delivery systems has to be able to control the release of highly volatile fragrances in functional perfumery products, and to

increase the stability of perfume raw materials (PRMs) with unstable chemical functional groups. The evaluation of the fragrance performance in consumer goods is a function of three empirical parameters: long-lastingness, substantivity, and diffusivity. These three factors refer to the property of a fragrance to be perceivable on a surface after several hours, the ability to smell that fragrance even after a drying process (*i.e.* in laundry application), and its capacity for being perceived at a further distance from its source during a reasonably long time period (as in air fresheners).<sup>8</sup>

Most perfumes start off their life as a liquid mixture for which perfumers do not know the exact composition of the headspace (defined as "the air or empty space left above the contents in a sealed container").<sup>9</sup> In order to gain a greater understanding of the nature of the vapour phase, and its relationship with the composition of the liquid phase, it is necessary to investigate the thermodynamic equilibria which define the phases. In other words it is necessary to measure the vapour-liquid equilibria (VLE) and liquid-liquid equilibria (LLE) of these rather complex mixtures. Headspace analysis is required to provide unambiguous analytical data. In this context, volatility is a key concept which can be defined as the "readiness to vaporise or evaporate, tendency to be readily diffused, or dissipated in the atmosphere, especially at ordinary temperatures",<sup>9</sup> and according to the functionalities of the molecule this process happens at different rates. According to this principle, fragrances can be classified as highly volatile (which have a vapour pressure greater than about 0.13 mbar at 25 °C), moderately volatile (between about 0.040 mbar to about 0.13 mbar), and poorly volatile (less than about 0.040 mbar). Based on the different amount of perfume raw materials in the vapour phase, the character of the fragrance can be composed of multiple notes.<sup>10</sup> For example, highly volatile molecules tend to smell citrusy, green, light and fresh, and they may be noticeable for only a few minutes after being applied to a substrate. In contrast, the moderately volatile PRMs are characterised by floral or fruity notes, which

<sup>a</sup>The QUILL Centre, The Queen's University of Belfast, Stranmillis Road, Belfast, UK, BT9 5AG.

<sup>b</sup>Procter & Gamble London Innovation Centre, Whitehall Lane, Egham, Surrey, UK, TW20 9NW.

<sup>c</sup>Procter & Gamble Brussels Innovation Centre, Temselaan 100, B - 1853, Strombeek-Bever, Brussels, Belgium.

† Footnotes relating to the title and/or authors should appear here.

Electronic Supplementary Information (ESI) available: [details of any supplementary information available should be included here]. See DOI: 10.1039/x0xx00000x

may be detectable for up to several hours. The poorly volatile compounds are typically sweet, musky or woody, and can last for several days. This variety of evaporation rates is not suitable for many fragrance compositions, and can limit the development of new perfumes. For example, the design of a fragrance with PRMs that evaporate in three hours after application has to be restricted to the highly volatile molecules characters. Creation of fragrance profiles is dominated by the moderately or poorly volatile perfume raw material characters. Thus, it is advantageous to be able to create fragrance compositions that span a wider range of fragrance characters, whilst still having all or substantially all of the scents evaporated within a given time frame.

The purpose of this current work is to describe the use of ionic liquids (which have no effective vapour pressure) as novel platforms for dissolving and releasing perfume raw materials, and to model their evaporation profile. The current work suggest a novel idea applicable to perfume product engineering,<sup>11</sup> and the structures have been selected with the target of human friendly media for consumer goods applications.

## Experimental

**Materials. Ionic liquid precursors.** The three new ionic liquids, namely (N-2-(2-methoxyethoxy)ethyl-N,N-dimethylethanaminium) 6-methyl-3,4-dihydro-1,2,3-oxathiazin-4-one 2,2-dioxide, [N<sub>112</sub>(2O2O1)][ace], (N-ethyl-2-(2-methoxyethoxy)-N,N-dimethylethanaminium) 1,4-bis(2-ethylhexoxy)-1,4-dioxobutane-2-sulfonate,

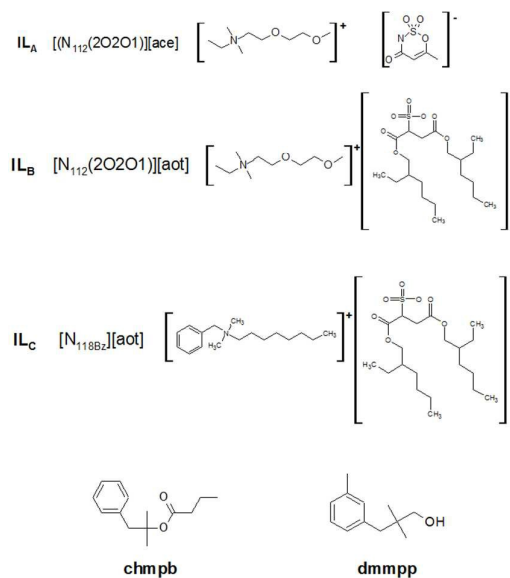


Figure 1. Structures of materials used in this work: (N-ethyl-2-(2-methoxyethoxy)-N,N-dimethylethanaminium) 6-methyl-3,4-dihydro-1,2,3-oxathiazin-4-one 2,2-dioxide, [N<sub>112</sub>(2O2O1)][ace]; (N-ethyl-2-(2-methoxyethoxy)-N,N-dimethylethanaminium) 1,4-bis(2-ethylhexoxy)-1,4-dioxobutane-2-sulfonate, [N<sub>112</sub>(2O2O1)][aot]; and N-benzyl-N,N-dimethyloctan-1-aminium 1,4-bis(2-ethylhexoxy)-1,4-dioxobutane-2-sulfonate, [N<sub>118Bz</sub>][aot]; (1-cyclohexyl-2-methylpropan-2-yl) butanoate, chmpb; and 2,2-dimethyl-3-(3-methylphenyl)propan-1-ol, dmmp.

[N<sub>112</sub>(2O2O1)][aot], and N-benzyl-N,N-dimethyloctan-1-aminium 1,4-bis(2-ethylhexoxy)-1,4-dioxobutane-2-sulfonate, [N<sub>118Bz</sub>][aot], were synthesised (vide infra) using the following reagents (ex. Aldrich, 99%) without further purification: 2-(2-methoxyethoxy)ethanol, thionyl chloride, pyridine, N,N-dimethylethylamine, N,N-dimethyloctylamine, benzyl chloride, sodium bis(2-ethylhexyl) sulfosuccinate, and potassium 6-methyl-1,2,3-oxathiazin-4(3H)-one 2,2-dioxide. Dichloromethane and methanol were dried over magnesium sulfate prior to use.

**Thermodynamics study.** The ionic liquids used in this work (see Figure 1) are: IL<sub>A</sub>, [N<sub>112</sub>(2O2O1)][ace]; IL<sub>B</sub>, [N<sub>112</sub>(2O2O1)][aot]; and IL<sub>C</sub>, [N<sub>118Bz</sub>][aot]. Other materials used include (1-cyclohexyl-2-methylpropan-2-yl) butanoate (chmpb), and 2,2-dimethyl-3-(3-methylphenyl)propan-1-ol (dmmp).

**Methods.** The ionic liquids IL<sub>A</sub>, IL<sub>B</sub>, and IL<sub>C</sub> were synthesised according to the schemes reported in Figures 2 and 3, and characterised using <sup>1</sup>H NMR spectroscopy, TGA, elemental analysis, and electrospray (ethanenitrile) mass spectrometry. The ionic liquids IL<sub>A</sub>, IL<sub>B</sub>, IL<sub>C</sub> and the molecules dmmp and chmpb were studied by examining the vapour-liquid equilibria (VLE) and liquid-liquid equilibria (LLE).

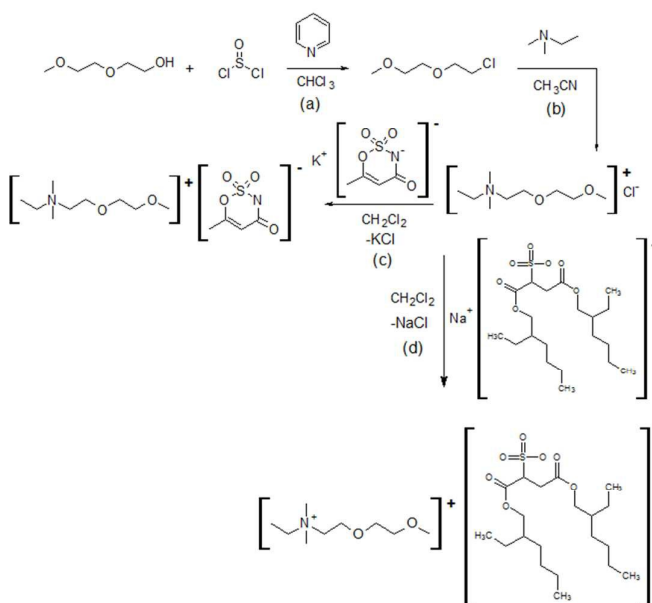


Figure 2. Synthetic scheme for the preparation of [N<sub>112</sub>(2O2O1)][ace] and [N<sub>112</sub>(2O2O1)][aot]: (a) synthesis of the chloroalkane, (b) quaternisation of the tertiary amine, and (c) and (d) anion metathesis.

**Synthesis of IL<sub>A</sub> and IL<sub>B</sub>.** (a)-Synthesis of 1-chloro-2-(2-methoxyethoxy)ethane. A solution of 2-(2-methoxyethoxy)ethanol (50.00 g, 0.416 mol) and pyridine (32.92 g, 0.416 mol) in dichloromethane (200 cm<sup>3</sup>) was added to a three-necked round-bottom flask fitted with a condenser under a dinitrogen flush. A solution of thionyl chloride (49.51 g, 0.416 mol) in dichloromethane was then added

dropwise over a period of 2 h to the stirred mixture *via* a pressure equalising funnel at room temperature. Once the addition was complete, the reaction mixture was then heated under reflux for 12 h. The reaction mixture was then cooled to room temperature, and washed with saturated aqueous sodium hydrogencarbonate (200 cm<sup>3</sup>), and then magnesium sulfate (5 g) was added to the organic phase. This mixture was then filtered and the filtrate was concentrated using a rotovaporator *in vacuo* at 40 °C to leave a pale yellow liquid. A simple distillation at 70 °C *in vacuo* produced a colourless liquid (56.02 g; 97% yield), which was used immediately in step (b).<sup>12</sup>

(b) - *Synthesis of (N-ethyl-2-(2-methoxyethoxy)-N,N-dimethylethanaminium) chloride*. A solution of the distilled 1-chloro-2-(2-methoxyethoxy)ethane (20.00 g, 0.144 mol), *N,N*-dimethylethylamine (10.55g, 0.144 mol; newly opened bottle) and dry methanol (50 cm<sup>3</sup>) was added in air to a screw cap glass tube. The mixture was then stirred (700 rpm) at 50 °C for 15 days. The mixture was cooled to room temperature and transferred to a rotovaporator, and the methanol and the excess of amine were removed under the reduced pressure. The orange residue was then washed with ethyl ethanoate (20 cm<sup>3</sup> x 3), cyclohexane (20 cm<sup>3</sup>, two times) and finally was concentrated using a rotovaporator *in vacuo* at 40 °C to leave a hygroscopic orange solid, which was subsequently dried *in vacuo* at 40 °C for 3 d (28.85 g, 93% of yield). Microanalysis: Calcd. C, 51.05; H, 10.47; N, 6.62: found C, 50.24; H, 10.6; N, 6.55; ES-MS (CH<sub>3</sub>CN): Calcd. M<sup>+</sup> 176.1651; found M<sup>+</sup> 176.1624.

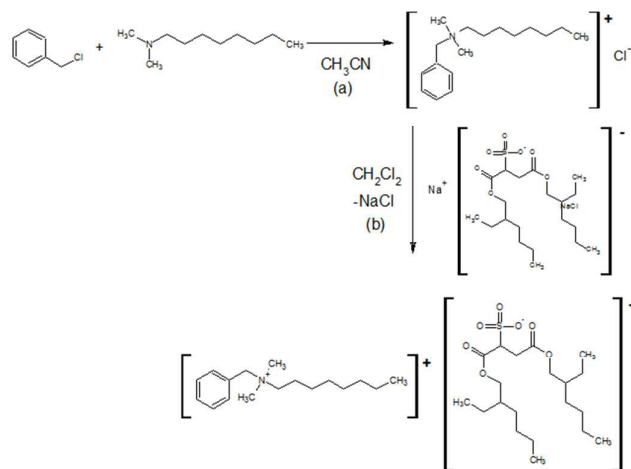


Figure 3. Synthetic scheme for the preparation of [N<sub>1.1.8.Bz</sub>][aot]: (a) quaternisation of the tertiary amine, and (b) anion metathesis.

(c) - *Synthesis of [N<sub>1.1.2</sub>(2O2O1)][ace]*. To a solution of the [N<sub>1.1.2</sub>(2O2O1)]Cl (10.00 g, 0.0472 mol) in dichloromethane (20 cm<sup>3</sup>), was added potassium acesulfamate (9.50 g, 0.0472 mol), and the mixture was stirred at room temperature for 2 d, whence it was centrifuged (3.5 rpm for 20 min) to remove the solid. The solvent was removed using a rotovaporator *in vacuo* at 40 °C to leave a pale yellow liquid, which was subsequently

dried *in vacuo* at 50 °C for 1 d (13.32 g, 83% of yield). Microanalysis: Calcd. C, 58.26; H, 9.95; N, 2.34; S, 5.36: found C, 57.01; H, 10.3; N, 2.27; S, 4.70 ES-MS (CH<sub>3</sub>CN): Calcd. M<sup>+</sup> 176.1651, M<sup>-</sup> 161.9861: found M<sup>+</sup> 176.1555, M<sup>-</sup> 161.9668.

(d) - *Synthesis of [N<sub>1.1.2</sub>(2O2O1)][aot]*. The same procedure was followed as for [N<sub>1.1.2</sub>(2O2O1)][ace], except that [N<sub>1.1.2</sub>(2O2O1)]Cl (10.00 g, 0.0472 mol) sodium docusate (21.00 g, 0.0472 mol) were used, yielding a pale yellow liquid (24.12 g, 85%). Microanalysis: Calcd. C, 58.26; H, 9.95; N, 2.34 S, 5.36: found C, 57.61; H, 9.88; N, 2.41; S, 5.26 ES-MS (CH<sub>3</sub>CN): Calcd. M<sup>+</sup> 176.1651, M<sup>-</sup> 421.2260 found: M<sup>+</sup> 176.1628, M<sup>-</sup> 421.2107.

#### Syntheses of IL<sub>c</sub>

(a) - *Synthesis of N-benzyl-N,N-dimethyloctan-1-aminium chloride*. A solution of the benzyl chloride (10.00 g, 0.0790 mol) and *N,N*-dimethyloctylamine (12.42 g, 0.0790 mol) was added to a screw cap glass tube. (The stirring speed was set at 500 RPM and the temperature was set at 50 °C). The reaction mixture was left in the sealed tube for 7 days before being stopped. The obtained orange mixture was washed with ethyl acetate, cyclohexane and concentrated via rotatory evaporator to yield a hygroscopic white solid, which was subsequently dried under high vacuum at 40 °C for 3 d. The final chloride ionic liquid was obtained in (24.12 g, 85%). Microanalysis: Calcd. C, 71.93; H, 10.65; N, 4.93: found C, 70.70; H, 10.99; N, 4.77; ES-MS (CH<sub>3</sub>CN): Calcd. M<sup>+</sup> 248.2378, found: M<sup>+</sup> 248.2375.

(b) - *Synthesis of [N<sub>1.1.8.Bz</sub>][aot]*. Sodium docusate (15.66 g, 0.0352 mol) was added to a solution of the chloride ionic liquid [N<sub>1.1.8.Bz</sub>][Cl] (10.00 g, 0.0352 mol) in dichloromethane (15 cm<sup>3</sup>). The reaction mixture was left stirring at room temperature for 2 d before being placed in the centrifuge. The potassium chloride by-product was filtered off and dichloromethane was concentrated to afford a viscous pale liquid as the desired product, which was then dried under high vacuum at 50 °C for 1d. The [N<sub>1.1.8.Bz</sub>][aot] was obtained in (21.56 g, 91%). Microanalysis: Calcd. C, 66.35; H, 10.08; N, 2.09 S, 4.79: found C, 66.55; H, 10.15; N, 2.19; S, 4.94 ES-MS (CH<sub>3</sub>CN): Calcd. M<sup>+</sup> 248.2378, M<sup>-</sup> 421.2260 found: M<sup>+</sup> 248.2366, M<sup>-</sup> 421.2606.

**Instrumental.** <sup>1</sup>H NMR spectra were recorded on a Bruker Avance III 400MHz spectrometer. ESMS-mass spectroscopy measurements were carried out on a Waters LCT Premier instrument with an Advion TriVersa Nano Mate injection system (cone voltage 50 V, source 120 °C). Both positive and negative ions were detected. Samples were injected as dilute solutions in ethanenitrile. DSC-scans (for melting point measurements) were obtained using a TA DSC Q2000 model with a TA Refrigerated Cooling System 90 (RCS). For each sample, three scans were run with scan rates of 5 °C min<sup>-1</sup>. Microanalysis: carbon, hydrogen, nitrogen and sulfur contents (wt%) were determined using a Perkin-Elmer Series II CHNS/O 2400 CHN Elemental Analyser, which provided values within 0.3 wt% error. Water content was determined using a Cou-Lo

Aquamax Karl-Fisher Moisture Meter (compact version 08.05). Ionic liquids were tested in duplicate immediately after drying under high vacuum for 24 h at 50 °C. The water content was less than 60 ppm for all samples.

Decomposition temperature measurements were performed using a TGA/DSC1 thermogravimetric analyser from Mettler-Toledo, Inc. The samples were measured in alumina crucibles, at a heating rate of 5 K min<sup>-1</sup> under a dinitrogen atmosphere. The onset of the weight loss in each thermogram was used as a measure of the decomposition temperature (point at 5 wt% loss of the sample). The melting points and glass transition temperatures of the synthesised compounds were measured by DSC, using a TA Instruments Modulated DSC Q 2000 V24.4 Build 116 with a refrigerated cooling system RCS 90 capable of controlling the temperature down to 220 K. Dry dinitrogen gas was purged through the DSC cell at a flow rate of ca. 20 cm<sup>3</sup> min<sup>-1</sup>.

**Determination of VLE. Calibration procedure:** All the FT-IR measurements reported were recorded using a PerkinElmer Spectrum 100 spectrometer, fitted with a Cyclone™ C5 series gas cell of volume 1.33 l. The cell was thermostatically controlled with an 8 m tuneable path length, and was linked to a vacuum pump (Edwards RV8).

Typically, prior to use, the cell was evacuated several times, alternating with dry dinitrogen flushes, until the infrared spectrum of the gas phase revealed the absence of any undesirable species. The sample was introduced into the cell and the evacuation process was started until the pressure dropped to 0.08 bar. The heating mantle was lowered over the cell, and the system was left equilibrating at a defined temperature. A spectrum was recorded periodically in order to check when the system had reached equilibrium, whence the absorbance was constant over time.

For each point of the calibration line, a defined quantity of chmpb was weighed. After recording the background, the weighed sample was introduced into the cell. The cell was then sealed, evacuated down to 0.08 bar, and then heated up to a temperature (150 °C) which ensured the complete evaporation of the sample for a defined equilibration time. Then the spectrum was recorded (15 scans at 10 spectra per second from 4000 to 1000 cm<sup>-1</sup>). The reproducibility was checked by repeating the spectral accumulation three times.

**Single component vapour pressure measurement.** In order to measure the concentration of chmpb in the vapour phase above the liquid sample, a defined and recorded quantity of the material was weighed into a vial and introduced into the FT-IR cell. The system was evacuated and thermostatically maintained at a defined temperature in order to reach equilibrium, and at this point the IR spectrum was recorded (see Figure 4). The two peaks considered for the quantification are those at 1746 cm<sup>-1</sup> (due to the CO stretching) and at 2980 cm<sup>-1</sup> (due to the CH stretching).

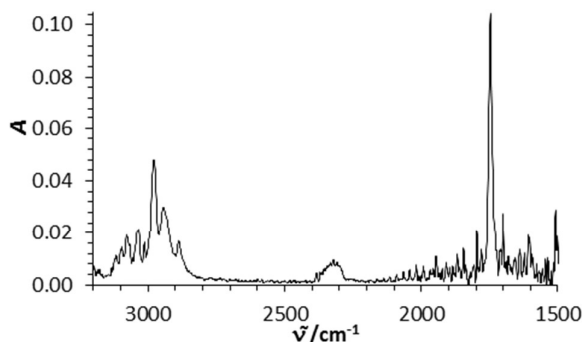


Figure 4. The gas phase IR spectrum (15 scans at 1 scan per 10 s from 4000 to 1000 cm<sup>-1</sup>) for chmpb at 30°C.

**Multicomponent systems:** The vapour pressure of the organic material chmpb in admixture with an ionic liquid (IL<sub>A</sub>, IL<sub>B</sub> or IL<sub>C</sub>) was measured using the same procedure reported for the single component. Here the vapour pressure has been expressed in terms of the relative concentration  $C_r$ , as defined in Equation (1).

$$C_r = \frac{A_{\text{mixture}}}{A_{\text{neat}}} \quad (1)$$

where  $C_r$  is the ratio between the absorbance of the chosen characteristic stretching mode, in the case of chmpb  $\nu_{\text{CO}}$ , in the ionic liquid mixture ( $A_{\text{mixture}}$ ) over the absorbance of the same stretching mode for the neat chmpb ( $A_{\text{neat}}$ ).

**Determination of kinetic of H<sub>2</sub>O uptake and saturation point.** The water content of the IL<sub>A</sub>, IL<sub>B</sub>, and IL<sub>C</sub> has been quantified using a Cou-Lo Aquamax Karl-Fisher Moisture Meter (compact version 08.05). The experiment consists of sampling each ionic liquid (1 g) left in an open vial during the first 12 h in order to establish a kinetic of absorption. The saturation points for these mixtures have been reached after 24 h of air exposure.

**Determination of LLE.** The cloud point of a material was used to measure the onset of liquid-liquid immiscibility. Cloud points were determined at atmospheric pressure using visual detection of the phase demixing (naked eye observation of turbidity followed by phase separation). Samples of the solutions were prepared in a closed Pyrex-glass vial with a stirrer inside.<sup>13</sup> Ternary phase diagrams were constructed from the cloud points of a mixture of an ionic liquid phase (with a defined water content of either 0.55 wt % or 8.00 wt %) - IL<sub>A</sub>, (0.1IL<sub>A</sub> + 0.9IL<sub>B</sub>),<sup>¶</sup> or (0.1IL<sub>A</sub> + 0.9IL<sub>C</sub>)<sup>¶</sup> - and two organic molecules chmpb and dmmpb (see Figure 1).

#### COSMO-RS for VLE prediction.

The calculation of the activity coefficient for mixtures of multicomponent systems involved two main steps: (a) the calculation of the lowest energy conformers of the molecules

<sup>¶</sup> Within this manuscript, the composition of ionic liquids mixtures is specified by weight fraction unless otherwise specified.

and ionic liquids using COSMO-conf, and (b) calculation of the average activity coefficients of these conformers of the multinary system of ionic liquids and the organic materials. The strength and nature of the interaction between the ionic liquids and the components involved is indicated by the calculated Raoult's plot from COSMO-therm, and estimating the area of the deviation from the ideal straight line. In the particular case involving ionic liquids, a *pseudo*-binary approach was used in the COSMO-therm program (Version C3.0 Release 14.01) to calculate the LLE and VLE of a mixture composed of an ionic liquid containing some water, with the cation and anion of the ionic liquid input as equimolar amounts of separate "compounds". The chemical potentials were calculated for the system (anion, cation and water), with the chemical potential of the ionic liquids as the sum of the chemical potentials of both the cation and anion. The COSMO-RS calculations and basis set parameterisation were performed at the BP/TZVP level (Turbomole,<sup>14</sup> DFT/COSMO with the BP functional and TZVP<sup>15</sup> basis set), using the fully optimised geometries at the same level of theory and parameter file BP TZVP C21 0025.

#### Olfactory tests.

In order to show the effect of the ionic liquids on the perception of fragrance profile in a fragrance composition, test compositions were made, and given to panellists of professional noses to evaluate.

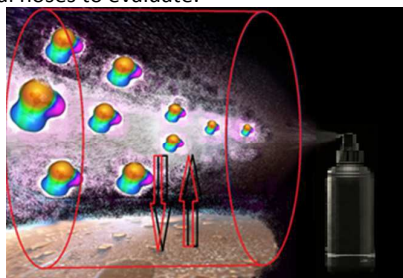


Figure 5. Glass slide perfume raw material as a VLE system.

At the testing facility, samples (50  $\mu$ L) of the fragrance compositions or the controls are applied to glass slides and placed on a hot plate at 32  $^{\circ}$ C to represent skin temperature (see Figure 5 for a schematic). Expert panellists were asked to assess the perceived fragrance profile (intensity and/or character) from each pair of samples, *i.e.*, that of the test composition *vs.* the corresponding control, at time 0 and later time points (*e.g.*, 1, 3, 6, 8 and up to 24 h post application) as the fragrance profile evolves. The panellists were asked to give a score on a scale of 0 to 5 for perceived fragrance intensity according to the odour intensity scale set out in Table 1.

Table 1. Odour Intensity Scale

Score	Fragrance Intensity	Score	Fragrance Intensity
0	Not detectable	3	Strong
1	Weak	4	Very Strong
2	Moderate	5	Overpowering

## Result and discussion

**Ionic liquid synthesis and characterisation.** The ionic liquids IL<sub>A</sub>, IL<sub>B</sub> and IL<sub>C</sub> (see Figure 1) were selected taking into account very preliminary and limited toxicology information.<sup>16</sup> For this reason, new-to-the world ionic liquids were designed to fit these criteria, and these are described in detail here. Although a similar study with [C<sub>4</sub>mim][NTf<sub>2</sub>] could have been performed, it would not have been applicable to consumer goods based on available toxicity data.<sup>17</sup> Clearly, for this study, a high degree of purity was required. The <sup>1</sup>H-NMR (see below) and ES-MS data confirmed the identity and purity of these novel liquids. In particular, the integration of the <sup>1</sup>H-NMR spectra confirmed the 1:1 molar ratio between the anion and the cation and the absence of organic impurities.

**1-chloro-2-(2-methoxyethoxy)ethane.** <sup>1</sup>H NMR ( $\delta_{\text{H}}$  / ppm, 400 MHz, CDCl<sub>3</sub>): 3.40(s, 3H); 3.57(m, 2H); 3.66(m, 4H); 3.76(m, 2H).

[N<sub>112</sub>(2O2O1)]Cl. <sup>1</sup>H NMR ( $\delta_{\text{H}}$  / ppm, 400 MHz, CDCl<sub>3</sub>): 3.98 (m, 2H, OCH<sub>2</sub>); 3.94 (m, 2H, OCH<sub>2</sub>); 3.80-3.79 (quartet, 2H, *J* = 4 Hz, NCH<sub>2</sub>); 3.67 (m, 2H, OCH<sub>2</sub>); 3.52 (m, 2H, OCH<sub>2</sub>); 3.42 (s, 6H, (NCH<sub>3</sub>)<sub>2</sub>); 3.36 (s, 3H, OCH<sub>3</sub>); 1.42 (t, 3H, CH<sub>3</sub>).

[N<sub>112</sub>(2O2O1)][ace], IL<sub>A</sub>. <sup>1</sup>H NMR ( $\delta_{\text{H}}$  / ppm, 400 MHz, CDCl<sub>3</sub>): 5.42 (s, 1H, CH[ace]); 3.94(m, 2H, OCH<sub>2</sub>); 3.71 (m, 2H, OCH<sub>2</sub>); 3.64-3.62 (m, 4H, (OCH<sub>2</sub>)<sub>2</sub>); 3.51 (m, 2H, NCH<sub>2</sub>); 3.34 (s, 3H, OCH<sub>3</sub>); 3.23 (s, 6H, (NCH<sub>3</sub>)<sub>2</sub>); 2.00 (s, 3H, (CH<sub>3</sub>) [ace]); 1.39 (t, 3H, (CH<sub>3</sub>)). *T<sub>g</sub>* = -66.6  $^{\circ}$ C.

[N<sub>112</sub>(2O2O1)][aot], IL<sub>B</sub>. <sup>1</sup>H NMR ( $\delta_{\text{H}}$  / ppm, 400 MHz, CDCl<sub>3</sub>)  $\delta$  4.12 (m, 1H, (CH) [aot]), 4.10-3.91 (m, 6H, (NCH<sub>3</sub>)<sub>2</sub>), 3.75 (s, 2H, (CH<sub>2</sub>) [aot]), 3.65 (m, 4H, (OCH<sub>2</sub>)<sub>2</sub>), 3.54 (s, 2H, NCH<sub>2</sub>), 3.38 (s, 3H, OCH<sub>3</sub>), 3.25 (s, 7H, (NCH<sub>3</sub>)<sub>2</sub>), 3.12 (m, 1H, (CH) [aot]), 1.74 (s, 2H, (CH<sub>2</sub>) [aot]), 1.65 (s, 1H, (CH) [aot]), 1.54 (s, 1H(CH) [aot]), 1.50-1.22 (m, 20H(CH<sub>2</sub>) [aot]), 0.89 (m, 12H, (CH<sub>2</sub>)<sub>6</sub> [aot]). *T<sub>g</sub>* = -81  $^{\circ}$ C.

[N<sub>118Bz</sub>]Cl. <sup>1</sup>H NMR ( $\delta_{\text{H}}$  / ppm, 400 MHz, CDCl<sub>3</sub>)  $\delta$  7.70-7.64 (m, 2H, *H*<sub>2,6</sub>), 7.50 - 7.40 (m, 3H, (ArCH)<sub>3</sub>), 5.09 (s, 2H, (NCH<sub>2</sub>Ph)), 3.56-3.48 (m, 2H, NCH<sub>2</sub>), 3.32 (s, 6H, (NCH<sub>3</sub>)<sub>2</sub>), 2.02 (m, 2H, (CH<sub>2</sub>)<sub>1</sub>), 1.29 (m, *J* = 20.5, 13.0 Hz, 10H(CH<sub>2</sub>)<sub>5</sub>), 0.88 (t, *J* = 6.8 Hz, 3H, (CH<sub>3</sub>)). *T<sub>m</sub>* = 62  $^{\circ}$ C.

[N<sub>118Bz</sub>][aot] IL<sub>C</sub>. <sup>1</sup>H NMR ( $\delta_{\text{H}}$  / ppm, 400 MHz, CDCl<sub>3</sub>)  $\delta$  7.58 (s, 2H, (*H*<sub>2,6</sub>), 7.44 (s, 3H, (Ar CH)<sub>3</sub>), 4.72 (s, 2H, (CH<sub>2</sub>-Ar)), 4.16 (m, 1H, (CH)<sub>1</sub> [aot]), 3.97 (m, 4H, N(CH<sub>2</sub>)<sub>2</sub>), 3.31 (m, 3H, (CH<sub>3</sub>), 3.15 (s, 7H, N(CH<sub>3</sub>)<sub>2</sub>, CH), 1.60 (s, 1H, (CH)<sub>1</sub> [aot]), 1.51 (s, 1H, (CH)<sub>1</sub> [aot]), 1.45-1.17 (m, 26H, (CH<sub>2</sub>) [aot]), 0.93 -0.79 (m, 15H, (CH<sub>2</sub>) [aot]). *T<sub>g</sub>* = -27.49 $^{\circ}$ C.

**VLE measurements. Calibration line and vapour pressure of single component (chmpb).** Infrared spectra of chmpb (see Figure 4) were recorded over the temperature range 25-40  $^{\circ}$ C. The absorbances of two specific stretching modes of chmpb ( $\tilde{\nu}_{\text{CO}} = 1746 \text{ cm}^{-1}$ ;  $\tilde{\nu}_{\text{CH}} = 2980 \text{ cm}^{-1}$ ) were selected, and plotted

against its concentration in the vapour phase (see Figure 6) and the data are reported in Table 2.

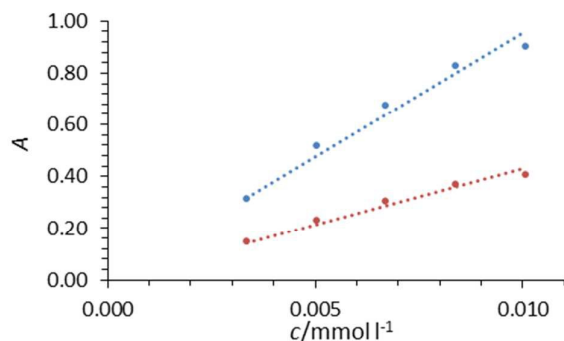


Figure 6. Beer-Lambert plots for chmpb. The data were fitted by linear regression and forced to go through the origin. For  $\bar{\nu}_{\text{CO}}$  (blue line), gradient =  $95300 \text{ l mol}^{-1}\text{cm}^{-1}$ ,  $R^2 = 0.9693$ ; for  $\bar{\nu}_{\text{CH}}$  (red line), gradient =  $42900 \text{ l mol}^{-1}\text{cm}^{-1}$  with  $R^2 = 0.9751$ . The standard deviation in  $A$  for the  $\bar{\nu}_{\text{CO}}$  is 0.0421, and for the  $\bar{\nu}_{\text{CH}}$  is 0.0152. The errors reflected in the standard deviations arise from the precision of the balance for weighing the samples.

Table 2. Calculated vapour pressure from the infrared absorbance of chmpb ( $\bar{\nu}_{\text{CO}} = 1746 \text{ cm}^{-1}$  and  $\bar{\nu}_{\text{CH}} = 2980 \text{ cm}^{-1}$ ) as a function of its gas phase concentration.<sup>a</sup>

$T/^\circ\text{C}$	$A_{\text{CH}}$	$P_{\text{CH}}/\text{kPa}$	$A_{\text{CO}}$	$P_{\text{CO}}/\text{kPa}$
25	0.0084	0.4846	0.0187	0.4861
30	0.0191	1.1205	0.0429	1.1338
35	0.0270	1.6101	0.0600	1.6119
40	0.0515	3.1209	0.1172	3.1998

<sup>a</sup>  $A$  and  $P$  are defined in Equations (2) to (4).

From the slope of the Beer-Lambert plot, Equation (2), reported in Figure 6, and using the ideal gas law, Equation (3),<sup>18</sup> the vapour pressure of the standard material has been calculated according to Equation (4) for each data set.<sup>19</sup>

$$A = \epsilon l c \quad (2)$$

$$PV = nRT \quad (3)$$

$$P = \frac{A}{\epsilon l} RT \quad (4)$$

where  $\epsilon$  = molar extinction coefficient,  $A$  = absorbance,  $l$  = path length (in cm),  $c$  = concentration (in  $\text{mol l}^{-1}$ ),  $P$  = pressure,  $V$  = volume,  $n$  = number of moles,  $R$  = gas constant and  $T$  = temperature.

The data reported in Table 2 clearly established the extinction coefficients for the two vibrational modes,  $\bar{\nu}_{\text{CO}}$  and  $\bar{\nu}_{\text{CH}}$ , as  $95300 \text{ l mol}^{-1}\text{cm}^{-1}$  and  $42900 \text{ l mol}^{-1}\text{cm}^{-1}$ , respectively. These were used to estimating the vapour pressure of chmpb at different temperatures. The two sets of calculated pressures match within an average error of 0.15 kPa. This is most likely due to the difficulty in controlling temperature inside the cell whilst the thermostat is on the heating jacket.

**Vapour pressure of chmpb in multicomponent mixtures.** The VLE of organic molecules in ionic liquids are essential data for describing the thermodynamics of these new mixtures. In the literature, the interactions between organic solvents and ionic liquids have been mostly evaluated using static methods,<sup>20</sup> which are useful and applicable for the study of organic molecules with relatively high vapour pressure. However, in this work, PRMs with low volatility were of interest, and so a newly developed method<sup>19</sup> was used. The VLE data are expressed as deviations from Raoult's law, and the observations are consistent with the nature of the interactions between organic molecules and ionic liquids, which have already been reported for fluorinated ionic liquids.<sup>21</sup>

The results of the study of the VLE of the systems composed of four different ionic liquid mixtures with chmpb are reported in Figures 7-10. All data deviate from the ideal linear Raoult's plot,<sup>18</sup> as represented by Equation (5).

$$P_i = P_i^0 \chi_i \quad (5)$$

where,  $P_i^0$  is the vapour pressure of the pure component at  $25^\circ\text{C}$ , and  $\chi_i$  is its mole fraction.

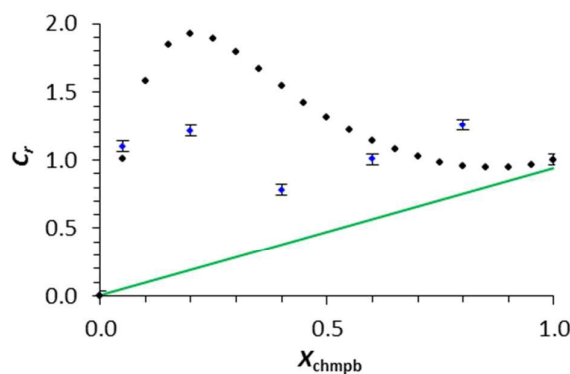


Figure 7. Vapour-liquid equilibria data of  $[\text{N}_{112}(\text{2O2O1})][\text{ace}]$  and chmpb mixtures at  $30^\circ\text{C}$  in blue, with the COSMO-therm calculations at  $30^\circ\text{C}$  represented in black and the ideal Raoult's plot in green.

The data reported for the system  $[\text{N}_{112}(\text{2O2O1})][\text{ace}]$  and chmpb show a pronounced positive deviation from ideality for this mixture. In particular, at low mole fraction (0.05) of chmpb, this behaviour suggests a strong mutual repulsion between the involatile ionic liquid and the volatile organic. The calculated values (COSMO-therm) for this mixture anticipate the strong repulsion observed in the experimental data, and also predict the maximum effect occurring at a mole fraction about 0.2.

The second ionic liquid tested,  $\text{IL}_B$ , has the same cationic structure, but the acesulfamate anion has been replaced with docusate anion, in order to increase the solubility of the hydrophobic organic molecules: VLE data are reported in Figure 8. Both empirically and computationally, the repulsive effect here is less than for  $\text{IL}_A$ , and there is a closer match between the theoretical prediction and the experimental observation.

In order to create a combination between the better solubility properties of the docusate anion and the greater repulsive effect of  $[N_{1,12}(2O2O1)][ace]$ , a mixture of the two ionic liquids has been studied. The mole ratio used was  $IL_A:IL_B = 1:1$  and the VLE data are given in Figure 9. It is evident that the deviation from Raoult's law for *chmpb* is a combination of the two curves shown in Figures 7 and 8, demonstrating consistency between the experimental and theoretical data.

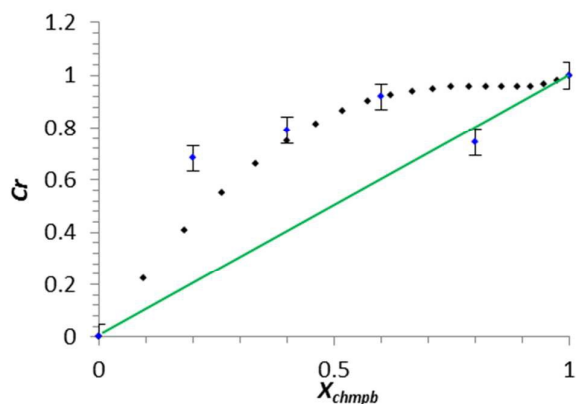


Figure 8. Vapour-liquid equilibria of  $[N_{1,12}(2O2O1)][aot]$  and *chmpb* mixtures at 45 °C in blue, COSMO-therm data in black at 45 °C and the ideal linear plot in green.

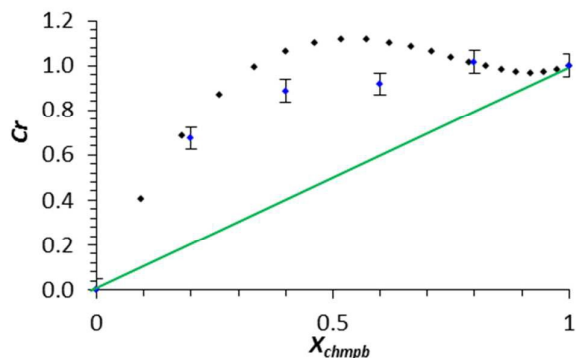


Figure 9. Vapour-liquid equilibria of a 1:1 ionic liquid mixture of  $[N_{1,12}(2O2O1)][ace]$  and  $[N_{1,12}(2O2O1)][aot]$  with *chmpb* at 45 °C in blue; COSMO-therm data in black and the ideal linear plot in green.

The fourth mixture tested was the ionic liquid  $[N_{1,18B2}][aot]$ ,  $IL_C$ , which has a docusate anion and a different type of cation, containing both a phenyl and an eight carbon chain and *chmpb*. The VLE plot (see Figure 10) shows a reduced repulsive effect compared to those obtained for  $IL_A$  and  $IL_B$ . This is most likely due to the presence of the aromatic ring, which will induce  $\pi$ - $\pi$  stacking of the cations within the liquid phase.

The calculated VLE data obtained using COSMO-therm are a qualitatively useful data set, and are able to predict the nature of the deviation from ideality, as reported for other organic molecules dissolved in ionic liquids.<sup>22</sup> However, the calculations are not quantitatively accurate in predicting the strength of the interactions between the solutes and ionic liquids, probably due to the presence of long range ion-ion interactions. However, for establishing trends

and predicting qualitative behaviour, this method has proved excellent.

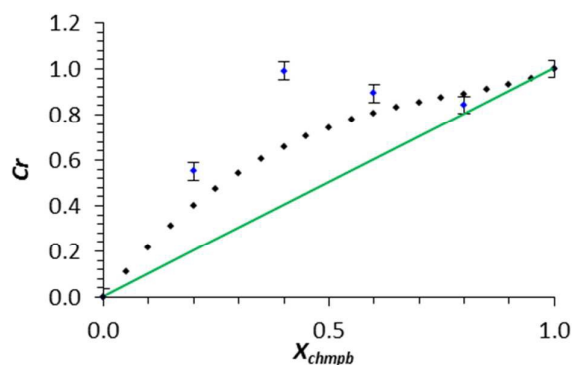


Figure 10. Vapour-liquid equilibria of the mixture  $[N_{1,18B2}][aot]$  and *chmpb* at 45 °C in blue, COSMO-therm data in black and the ideal linear plot in green.

**Kinetics of water uptake and saturation.** The ionic liquids reported in Figure 1 and their mixtures, due to their structures, are hygroscopic and so tend to absorb water if left in the open air (see Figure 11). The water uptake of room temperature ionic liquids has been widely investigated,<sup>23</sup> and the kinetics of absorption have been already reported for a few systems.<sup>24</sup> The amount of water absorbed is, *inter alia*, a function of the cationic and anionic structures, and the time of exposure.

This, of course, will be the realistic situation of any application of a consumer product. In all cases the ionic liquids absorb water from the atmosphere, initially approximately proportionate to their exposure time (see inset on Figure 11), but each as a different rate. After 24 h, all the ionic liquids appeared to have reached equilibrium, and all showed a significant water content.

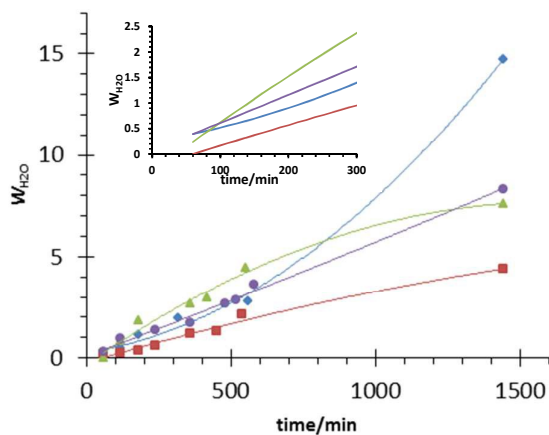


Figure 11. Water uptake of ionic liquids, measured by Karl-Fischer titration, as a function of time: in blue diamond  $IL_A$ , in red squares  $IL_B$ , in green triangle the mixture (0.9  $IL_A$  + 0.1  $IL_C$ ) and in purple circle the mixture (0.9  $IL_A$  + 0.1  $IL_B$ ). The inset represents a simplified expansion of the absorption between 0-300 min.

The water uptake of the  $IL_A$ ,  $IL_B$  and  $IL_C$  and two mixtures (0.9  $IL_A$  + 0.1  $IL_B$  and 0.9  $IL_A$  + 0.1  $IL_C$ ) has been studied titrating the water content in time and the results are the kinetic of the

water absorption and as final value the saturation point has been reported occurring after 24 h of atmospheric exposure. Fortuitously, the presence of water has a moderating effect on the vapour pressure of the mixture. This is demonstrated by the deliberate addition of precise amount of water to solutions of chmpb in IL<sub>A</sub>, IL<sub>B</sub> and IL<sub>C</sub>, as well as to mixtures of IL<sub>A</sub>, IL<sub>B</sub> and IL<sub>C</sub> (see following section).

**Liquid-liquid equilibria measurements.** The interactions of ionic liquids containing dissolved organic materials with water have been studied previously,<sup>25</sup> and phase separation was observed to occur. An insolubility gap is defined as the "area within the coexistence curve of an isobaric phase diagram (temperature vs composition) or an isothermal phase diagram (pressure vs composition)"<sup>26</sup> and, the physicochemical observations are consistent with this phenomenon. The strength of the interactions involved are mainly driven by the structures of the ionic liquids and the organic molecules.

The LLE data for IL<sub>A</sub>, IL<sub>B</sub> and IL<sub>C</sub> and their mixtures reveals a region in the ternary phase diagram, delimited by the points of the binodal line (defined by the black and red data series of cloud points), where the two organic species (chmpb and dmmpp) are insoluble in the ionic liquid mixtures. From the data reported in the first ternary phase diagram (Figure 12) for the components IL<sub>A</sub>, chmpb and dmmpp (recorded as mole fraction on the three axes); it is clear that IL<sub>A</sub> is the key component responsible for the water uptake. For example during the first 12 h, when it reached the 8 wt<sub>H2O</sub> %, the insolubility gap defined by the red data series is increased compared with the dried IL<sub>A</sub> mixture (black data series).<sup>23</sup>

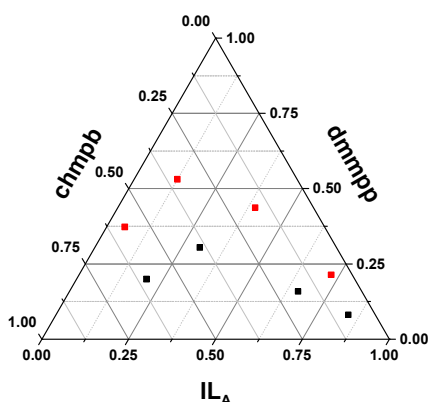


Figure 12. Ternary phase diagram of IL<sub>A</sub> [N<sub>1,1,2</sub>(2O2O1)][ace] with dmmpp and chmpb. The black series of data defines the binodal line of a mixture with 0.2 wt<sub>H2O</sub> %. The red series of data defines the binodal line of a mixture with 8 wt<sub>H2O</sub> %.

In order to increase the solubility of chmpb in IL<sub>A</sub>, 10 wt% of one of the other two ionic liquids (IL<sub>B</sub> or IL<sub>C</sub>) has been added to the mixture, and the results are reported in Figures 13 and 14. Again, in these cases, the water uptake increases the area of the insolubility region.

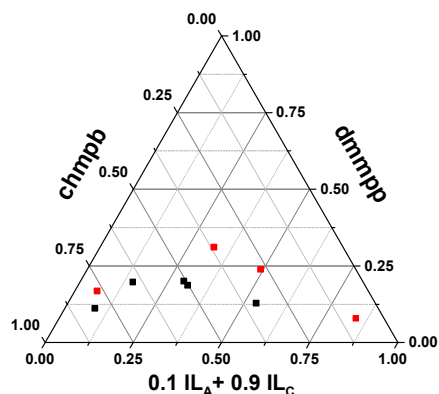


Figure 13. Ternary phase diagram of the ionic liquid mixture (0.1 IL<sub>A</sub> + 0.9 IL<sub>C</sub>) with dmmpp and chmpb. The black series of data defines the binodal line of a mixture with 0.2 wt<sub>H2O</sub> %. The red series of data defines the binodal line of a mixture with 8 wt<sub>H2O</sub> %.

The enhancement in the solubility gap between the wet mixture (8 wt<sub>H2O</sub> %) and the dry one (0.2 wt<sub>H2O</sub> %) is mainly due to the effect of the cation. In Figure 13, the solubility gap for a possible real dry mixture (represented by black dots) has an acceptable composition range, usable in a homogeneous solution of ionic liquids and organic components mixtures (VLE data previously reported). At the same time, the repulsive effect is represented by the positive deviation from Raoult's law reported in Figures 7-10.

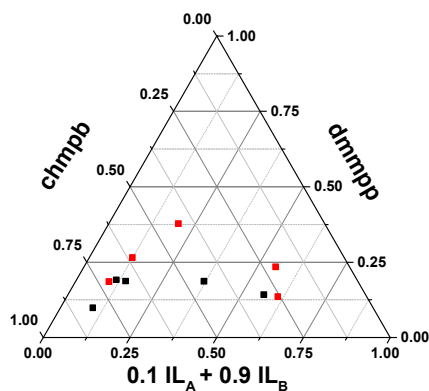


Figure 14. Ternary phase diagram of the ionic liquid mixture (0.1 IL<sub>A</sub> + 0.9 IL<sub>B</sub>) with dmmpp and chmpb. The black series of data defines the binodal line of a mixture with 0.2 wt<sub>H2O</sub> %. The red series of data defines the binodal line of a mixture with 8 wt<sub>H2O</sub> %.

**Olfactory Tests.** The ionic liquids mixtures IL<sub>A</sub> and IL<sub>B</sub> were tested in accordance with the protocol described above, and the olfactive profile, strength and character, of the PRMs in an open system was evaluated (see Table 3). All formulations contain 5 wt% of the chmpb, which imparts a character which varies from a fruity prune note when very concentrated, through harsh green as it becomes less concentrated and to a sweeter green note when at lower concentration. In formulation A, the PRM is solubilised in a traditional perfumery

solvent, dipropylene glycol (dpg), and a very strong fragrance strength is perceived from the start that only falls by 1 unit after three hours, and is still perceived as moderate in strength for up to 24 hours. The character also retains a fairly constant harsh green note for the first 5 hours. In formulation B, the same amount of the PRM is present in the ionic liquid mixture. In this case, the initial strength is greater by 1 unit compared to formulation A. This initial over-powering strength is maintained for the first 3 hours and drops by only 1 unit over five hours, clearly demonstrating the increased level of the PRM in the air as a result of the repulsion effect of the ionic liquid. After 24 hours, the odour from the ionic liquid solution of chmpb is much weaker, demonstrating the repulsion effect of the ionic liquid where the perfume material has been exhausted.

Table 3. Results of olfactory test on two samples: Sample A is a mixture of dipropylene glycol (dpg) and (chmpb); In Sample B, the dpg was replaced with the ionic liquid mixture 52.5:42.5 wt% [N<sub>112</sub>(2O2O1)][ace] (IL<sub>A</sub>) and [N<sub>112</sub>(2O2O1)][aot] (IL<sub>B</sub>).

Formulation	Time After Application				
	10 min	1 h	3 h	5 h	24 h
A: 5 wt% chmpb in 95 wt% DPG	4.0	4.0	3.0	3.0	2.0
	Harsh green	Harsh green	Harsh green	Harsh green	Sweeter green
B: 5 wt% chmpb in 52.5 wt% IL <sub>A</sub> & 42.5 wt% IL <sub>B</sub>	5.0	5.0	5.0	4.0	1.5
	Very fruity, prune	Very fruity, prune	Very fruity, prune	Very fruity, prune	Very weak, fruity

**COSMO-RS predictions.** COSMO-RS (Conductor-like screening model for real solvents), proposed by Klampert,<sup>27</sup> allows a theoretical description of a system composed of ionic liquids (ionic) and organic molecules (molecular). This methodology, once evaluated against empirical data, will allow the determination of phase diagrams and VLE data for multicomponent mixtures far more easily and rapidly than any experimental programme. For this reason, three-component mixtures containing one organic species, one ionic liquid, and water were examined both computationally and empirically, in order to evaluate the validity and usefulness of the COSMO-RS predictions.

The empirical vapour-liquid equilibria data for IL<sub>A</sub>, IL<sub>B</sub>, and IL<sub>C</sub> with chmpb (see Figures 8, 9 and 11, respectively) are reported, along with the predictions from the COSMO-therm calculations. Within the errors of the experimental data (which in some cases are considerable owing to the low vapour pressure of chmpb), the agreement is about 20%. More significantly, the calculated data show the same trend as the experimental data, and reproduce both the sign of the deviation from linearity in the Raoult's plots and the shape and position of the observed maxima. In other words the

predictions have value in that they reproduce reality qualitatively, but not quantitatively.

Table 4: Raoult's deviation plot area ( $A_d$ ) calculated using a Simpson integration method.<sup>28</sup> The data were reported in the first column for the dry mixture of each perfume raw material listed here with the ionic liquid [N<sub>112</sub>(2O2O1)][ace], and in the second column for the wet mixture (same composition but with 10 wt% H<sub>2</sub>O).

Organic materials	$A_d$ (dry)	$A_d$ (with 10% H <sub>2</sub> O)
Adoxal	0.86	2.26
Ambercore	0.50	1.53
Ambrocenide	0.97	2.87
a-amyl cinnamaldehyde	0.80	2.06
Apritone	0.64	1.59
Butylundecylate	1.14	3.59
Cyclohexadecenone	0.81	2.20
d-Musconone	1.06	2.92
Exaltenone	0.66	1.63
Fixolide	0.66	1.69
Frutene	0.75	1.82
Galaxolide	0.97	2.65
Geranylglucate	0.87	2.32
Glycollierral	0.72	1.75
Hexalon	0.70	1.79
Hexyl cinnamaldehyde	0.72	1.69
Iso-E-SuperR	0.76	1.98
Linalyl Cinnamate	0.75	1.85
Musconone	0.78	2.15
Muscogene	0.78	2.09
Nectaryl	0.74	1.89
Nerolidol	0.71	2.05
Norlimbanol	0.77	2.42
OkoumalR	0.95	2.68
Pharone	0.68	1.55
Timberol	0.77	2.42
Vertofix	0.71	1.97
Z-ambrettolide	0.83	2.24

Having established the general utility of the model and its application to a large set of organic fragrances (see Table 4), the COSMO-RS model has been used to classify the strength of the interaction between perfume raw material and the ionic liquid. Manipulation of a large database of molecules, required for studying commercial fragrance products, was performed in the past using large sets of experimental data connected with the arbitrary split of molecular structures in their functional group constituents.<sup>29</sup> The experimental data available for the system previously described are not sufficient for using a group contribution method such as UNIFAC, and for this reason a quantum chemical calculation model COSMO-RS (Conductor like Screening Model for Real Solvents)<sup>27</sup> has been applied. The proof of principle for this controlled fragrance release system has been demonstrated using a mixture of a perfume raw material, a co-solvent, and one of three ionic liquids, but is clear that a real mixture would involve an increased number of components.

The LLE data previously reported defined the effect of the water uptake in the solubility of the chmpb in the ionic liquid

mixtures. Here we demonstrate that a greater insolubility region in the ternary phase diagram (see Figures 13-15) is reflected by an increased deviation from Raoult's law. Computationally, the strength of the "salting out" effect, due to the ionic liquid's water uptake, can be represented as the area of deviation from Raoult's plot calculated using the Simpson's method (see Table 4).<sup>28</sup> The data reported show the increase in the Raoult's deviation area values for a selected list of hydrophobic perfume raw materials in the ionic liquid [N<sub>1,12</sub>(2O2O1)][ace]. The activity coefficients of the chmpb, calculated using COSMO-RS, suggest that the presence of water enhances the values, probably because of the chaotropic effect<sup>30</sup> of water in this system.

## Conclusions

A new way to release organic material into the gas phase with an enhanced vapour pressure has been described, the organic material exhibiting positive deviations from Raoult's law. The system involves dissolving the organic in an ionic liquid, which itself exhibits negligible vapour pressure. Moreover, utilising the custom design, which is a fundamental precept of ionic liquid chemistry, the novel ionic liquids used in this study were specifically designed to be toxicologically safe, and detailed synthetic procedures have been reported.

In a study of the liquid-liquid equilibria of (1-cyclohexyl-2-methylpropan-2-yl) butanoate in all four ionic liquids, it was surprising to discover that the addition of water (which will be omnipresent in a practical application of this new phenomenon) enhanced the vapour pressure of the ester. This observation suggests that the enhanced volatility of fragrances is not just a function of their intrinsic volatility, but also depends on the strength of the chaotropic interaction with the ionic liquid, and indeed with the organic component itself.

Given the large number of known and predictable ionic liquids, it is not feasible to screen all the possible options of both solute and solvent. For this reason, a computational approach based on a solvation model (COSMO-RS) was investigated in order to compute the nature and the strength of the interaction between the solute and the solvent. This rapid and easily accessible methodology revealed a remarkable qualitative agreement with the experimental data in both the direction and the maximum effect for the Raoult's law deviation, but was less successful in predicting its magnitude. Moreover, the methodology was simply applicable to multicomponent systems, providing invaluable guidance to minimise the number of experimental determination required to find optimal conditions.

## Acknowledgements

F.M.F.V. wishes to thank the EPSRC and Procter & Gamble for the award of a doctoral studentship.

## Author information

E-mail: quill@qub.ac.uk

## Notes and references

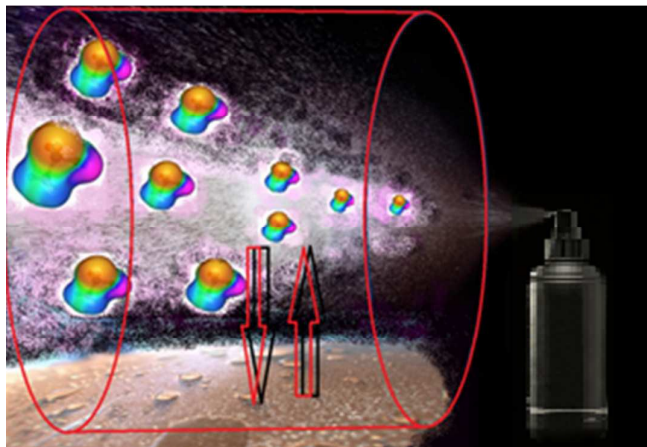
1. M. Freemantle, *An introduction to ionic liquids*, Royal Society of Chemistry, Cambridge, 2010.
2. P. Davey, *Perfumer and Flavorist*, 2008, **33**, 34-35.
3. F.-M. Petrat, F. Schmidt, B. Stutzel and G. Kohler, US Pat., 20060166856 A1, 2003.
4. (a) M. Blesic, H. Q. N. Gunaratne, P. Nockemann, P. McCarron and K. R. Seddon, *RSC Adv.*, 2013, **3**, 329-333; (b) H. Q. N. Gunaratne, P. Nockemann and K. R. Seddon, *Chem. Commun.*, 2015, **51**, 4455-4457.
5. (a) D. M. Bourgeois, G. S. Miracle, P. J. Porter, E. Boros, K. R. Seddon and H. Q. N. Gunaratne, US Pat., 8093432 B2, 2012; (b) Y. G. Aouad, D. M. Bourgeois, G. S. Miracle, J. Wevers, H. Q. N. Gunaratne, K. R. Seddon, E. Boros, S. P. Katdare and T. Belhocine, US Pat., 7414158 B2, 2008.
6. S. A. Forsyth, H. Q. N. Gunaratne, C. Hardacre, A. McKeown, D. W. Rooney and K. R. Seddon, *J. Mol. Catal. A*, 2005, **231**, 61-66.
7. K. Glendenning and M.-C. Dillon, eds., *British Perfumery: A Fragrant History*, British Society of Perfumers, Frome, 2013.
8. T. Stora, S. Escher and A. Morris, *CHIMIA Int. J. Chem.*, 2001, **55**, 406-412.
9. in *Oxford English Dictionary*, 2016.
10. C. S. Sell, *Chemistry and the Sense of Smell*, John Wiley & Sons, Ashford Kent, 2<sup>nd</sup> edn., 2014.
11. V. G. Mata, P. B. Gomes and A. E. Rodrigues, *AIChE J.*, 2005, **51**, 2834-2852.
12. D. A. Gedefaw, Y. Zhou, Z. Ma, Z. Genene, S. Hellström, F. Zhang, W. Mammo, O. Inganäs and M. R. Andersson, *Polym. Int.*, 2014, **63**, 22-30.
13. J. R. Trindade, Z. P. Visak, M. Blesic, I. M. Marrucho, J. A. P. Coutinho, J. N. Canongia Lopes and L. P. N. Rebelo, *J. Phys. Chem.*, 2007, **111**, 4737-4741.
14. (a) R. Ahlrichs, M. Bär, M. Häser, H. Horn and C. Kölmel, *Chem. Phys. Letters*, 1989, **162**, 165-169; (b) A. Schäfer, A. Klamt, D. Sattel, J. C. Lohrenz and F. Eckert, *Phys. Chem. Chem. Phys.*, 2000, **2**, 2187-2193.
15. A. Schäfer, C. Huber and R. Ahlrichs, *J. Chem. Phys.*, 1994, **100**, 5829-5835.
16. L. A. M. Holland, O. Todini, D. M. Eike, J. M. Velazquez Mendoza, S. A. Tozer, P. M. McNamee, J. R. Stonehouse, W. E. Staite, H. C. R. Fovargue, J. A. Gregory, K. R. Seddon, H. Q. N. Gunaratne, A. V. Puga, J. Estager, F.-L. Wu, S. D. Devine, M. Blesic and F. M. Ferrero Vallana, WO Pat., 2016049390 A1, 2016.
17. M. Petkovic, K. R. Seddon, L. P. N. Rebelo and C. S. Pereira, *Chem. Soc. Rev.*, 2011, **40**, 1383-1403.
18. P. Atkins and J. De Paula, *Elements of Physical Chemistry*, Oxford University Press, Oxford, 2<sup>nd</sup> edn., 2013.
19. F. M. Ferrero Vallana, L. A. M. Holland and K. R. Seddon, *Aust. J. Chem.*, 2016, DOI: <http://dx.doi.org/10.1071/CH16151>, -.
20. A. Heintz, T. V. Vasiltsova, J. Safarov, E. Bich and S. P. Verevkin, *J. Chem. Eng. Data*, 2006, **51**, 648-655.
21. M. B. Shiflett, M. A. Harmer, C. P. Junk and A. Yokozeki, *Fluid Phase Equilib.*, 2006, **242**, 220-232.
22. M. G. Freire, L. M. Santos, I. M. Marrucho and J. A. Coutinho, *Fluid Phase Equilib.*, 2007, **255**, 167-178.

## Journal Name

## ARTICLE

23. K. R. Seddon, A. Stark and M. J. Torres, *Pure Appl. Chem.*, 2000, **72**, 2275-2287.
24. C. D. Tran, S. H. D. P. Lacerda and D. Oliveira, *Appl. Spectrosc.*, 2003, **57**, 152-157.
25. M. G. Freire, A. F. M. Claudio, J. M. Araujo, J. A. Coutinho, I. M. Marrucho, J. N. C. Lopes and L. P. N. Rebelo, *Chem. Soc. Rev.*, 2012, **41**, 4966-4995.
26. W. J. Work, K. Horie, M. Hess and R. F. T. Stepto, *Pure Appl. Chem.*, 2004, **76**, 1985.
27. A. Klamt, *J. Phys. Chem.*, 1995, **99**, 2224-2235.
28. C. W. Clenshaw and A. R. Curtis, *Num. Math.*, 1960, **2**, 197-205.
29. S. I. Sandler, *Chemical and engineering thermodynamics*, New York 3rd edn., 1998.
30. H. Zhao, *J. Chem. Tech. and Biotech.*, 2006, **81**, 877-891.

## TOC



The vapour-liquid equilibria of organic molecules dissolved in ionic liquids revealed positive deviation from Raoult's law, especially with added water.